WORKSPACE OF WIRE-ACTUATED PARALLEL MANIPULATORS AND VARIATIONS IN DESIGN PARAMETERS

Vahid Nazari, Leila Notash
[1]*Department of Mechanical and Materials Engineering, Queen's University, Kingston, Canada*
E-mail:notash@me.queensu.ca; nazariv@me.queensu.ca

Received November 2012, Accepted March 2013
No. 12-CSME-104, E.I.C. Accession 3424

ABSTRACT

The purpose of the paper is to investigate the effect of small variations (uncertainties) and large variations in design parameters on the size and shape of the workspace of the wire-actuated parallel manipulators. The static force/moment balance equations, taking into account the null space of the Jacobian matrix, are used for the workspace analysis. The parameters examined include: the winding direction of wires on the pulleys; the radius of the pulley; the orientation, radius, and mass of the mobile platform; the peg length; and the ratio of the peg radii at the entrance and exit. Also, the effect of the geometric arrangement of wire attachment points and the number of wire connection points on the mobile platform, on the size and shape of the workspace is considered. The simulation results show the effect of small and large variations in the aforementioned parameters on the workspace of wire-actuated parallel manipulators without and with gravity.

Keywords: wire-actuated parallel manipulators; workspace analysis; parameters variations.

L'ESPACE DE TRAVAIL DES MANIPULATEURS PARALLÈLES À CABLES ET LES VARIATIONS DANS LES PARAMÈTRES DE CONCEPTION

RÉSUMÉ

Le but de cet article est d'investiguer, dans les paramètres de conception, les effets des petites variations (incertitudes), de même que les plus grandes, sur la dimension et la forme de l'espace de travail des manipulateurs parallèles à câbles. Les équations d'équilibre force/moment statique sont utilisées pour analyser l'espace de travail, tout en tenant compte de la zone morte de la matrice jacobienne. Dans les paramètres examinés ont été inclus : la direction de l'enroulement des câbles sur les poulies; le rayon de la poulie, l'orientation, le rayon et la masse de la plateforme mobile; la longueur de l'ancrage; et le ratio des rayons à l'entrée et à la sortie. Également considéré est l'effet sur la dimension et la forme de l'espace de travail de l'arrangement géométrique des points d'attache des câbles et le nombre de points d'attache sur la plateforme mobile. Les résultats de la simulation montrent l'effet des petites et grandes variations dans les paramètres mentionnés ci-dessus sur l'espace de travail des manipulateurs parallèles avec ou sans gravité.

Mots clés : manipulateurs parallèles actionnés par câbles; analyse de l'espace de travail; variation des paramètres.

1 INTRODUCTION

Determination of the reachable workspace of manipulators plays an important role in the design and analysis of robot manipulators. Workspace is the set of positions and orientations (poses) that the end-effector (mobile platform) of the manipulator can reach. Parallel manipulators are closed-loop mechanisms in which the mobile platform is generally connected to the base platform by means of a number of kinematic chains of links and joints. Parallel manipulators consist of a base platform, a mobile platform, and legs which connect the base platform to the mobile platform. In wire-actuated parallel manipulators, the solid-link legs are replaced by wires. That is, in these types of manipulators the pose of the mobile platform is controlled via wires. The light weight, high load capacity, large workspace, and simpler dynamic model are some advantages of wire-actuated parallel manipulators compared to solid-link parallel manipulators [1-2]. However, one considerable drawback is that wires can only exert tensile force and cannot push on the mobile platform. Therefore, at least $n + 1$ wires are necessary in order to fully control an n degrees of freedom wire-actuated parallel manipulator [3]. For example, in planar wire-actuated parallel manipulators with two translations on the plane and a rotation about the axis perpendicular to the plane of motion, at least four wires are required to fully control the pose of the mobile platform. Examples of these manipulators can be seen in Fig. 1 and Fig. 2.

Many studies have been conducted pertaining to the design and workspace analysis of wire-actuated parallel manipulators [4–6]. The workspace of wire-actuated parallel manipulators is a set of positions where the operation point (e.g., center of the mass) of the mobile platform can be located as long as all wires remain in tension for a given mobile platform orientation. Various workspace analysis methods have been utilized for wire-actuated parallel manipulators. The null space of the Jacobian matrix of the manipulators was used in [2, 7–9] for the discrete solution of the workspace, based on the formulation of wire tension. Using this method, the minimum and maximum allowable wire tensions can be taken into account. In addition, in [10–11] convex hull theory was utilized for the discrete solution to the force-closure workspace of these manipulators. Analytical solution to define the borders of the workspace of the planar wire-actuated parallel manipulator was investigated in [12–14]. The Antipodal method from multi-finger grasping was applied in [14] to determine the wrench-closure workspace of planar wire-actuated parallel manipulators.

In [15], the optimal design of 6–6 wire-actuated manipulators was analyzed, i.e., the largest workspace and global condition number of Jacobian matrix were investigated for different geometry, size and orientation of the mobile platform. In [16], the largest dexterous workspace (a set of positions where the operation point of the mobile platform can be located for all orientations) of planar wire-actuated parallel manipulators in terms of the number of wires, load, and orientation of the mobile platform was investigated. The workspace of the wire-actuated parallel manipulators, taking into account the uncertainty in the wire connections, was studied in [17] and the geometric representations of the uncertainties in the wire attachment points to the base and to the mobile platform were developed. It was proven that a small difference in the diameters of the wire and peg hole at the wire connections could lead to significant change in the workspace when compared to the results with no uncertainty. Although there are various works on the workspace of the wire-actuated parallel manipulators, the effect of uncertainties and variations in design parameters on the workspace has not been investigated comprehensively. Different values of design parameters will result in different area and shape for the workspace of wire-actuated parallel manipulators. As well, the exact values of some parameters of these manipulators are not known. Therefore, knowledge on how the design parameter variations could affect the performance of wire-actuated manipulators could be very valuable during their design and operation.

In this paper, the workspace of the planar wire-actuated parallel manipulators is generated by means of the formulation of static force/moment balance equations. The objective of the paper is to investigate the effect of the small variations (uncertainties) and the large variations in design parameters on the

workspace of the wire-actuated parallel manipulators. Specifically, the winding direction of wire on the pulley; the radius of the pulley; the orientation, radius, and mass of the mobile platform; the length of wire attachment peg on the mobile platform; the ratio of the peg radii at the entrance and exit; and the geometric arrangement of wire attachment points on the mobile platform are examined. The organization of this paper is as follows. In Section 2, the kinematic modeling of wire-actuated parallel manipulators is presented, including the wire attachment points to the mobile platform and to the pulley. Conditions for wire bending at the exit point of the attachment peg are also discussed. In Section 3, the static force/moment balance equations are derived to analyze the workspace of the manipulators. In Section 4, the effect of variations in design parameters on the workspace of a selected layout is presented. Finally, discussion and conclusion is given in Section 5.

2 KINEMATIC MODELING

In wire-actuated parallel manipulators, the wires connect the mobile platform to the base. That is, the wires are attached to the mobile platform at one end and are pulled with motors from the other end. To accurately control the mobile platform pose, a pulley is placed between the motor and the mobile platform. The wire release point on the pulley is referred to as the anchor position and the wire attachment point to the mobile platform is termed as the wire attachment peg. As the mobile platform pose is changed, the anchor position varies.

There are variations of wire-actuated parallel manipulators based on the number of wires, the arrangements of wire connections on the mobile platform, the winding direction of wires on the pulleys, position of the pulleys, and the shape of the mobile platform. In Fig. 1 and Fig. 2, two types of wire-actuated parallel manipulators according to the arrangements of wire connections on the mobile platform are presented. In Fig. 1, the wires are connected to distinct points on the mobile platform (4-4 wire layout), whereas in Fig. 2, two wires share the same attachment point (2-4 wire layout). Each type is classified into three different configurations based on the winding direction of wires over pulleys, i.e., clockwise or counter-clockwise direction. In Fig. 1(a) and Fig. 2(a), the winding of wires 1 and 3 and wires 2 and 4 around their corresponding pulleys are in the same direction. These winding directions of wires on the pulleys result in a symmetric manipulator. In Fig. 1(b) and Fig. 2(b), wires 1, 2 and 4 are wound in the same direction and wire 3 is wound in the opposite direction. In Fig. 1(c) and Fig. 2(c), all four wires are wound in the same direction. Unlike the manipulators of Fig. 1(a) and Fig. 1(b), the last two manipulators are asymmetric according to the winding direction of wires on the pulleys.

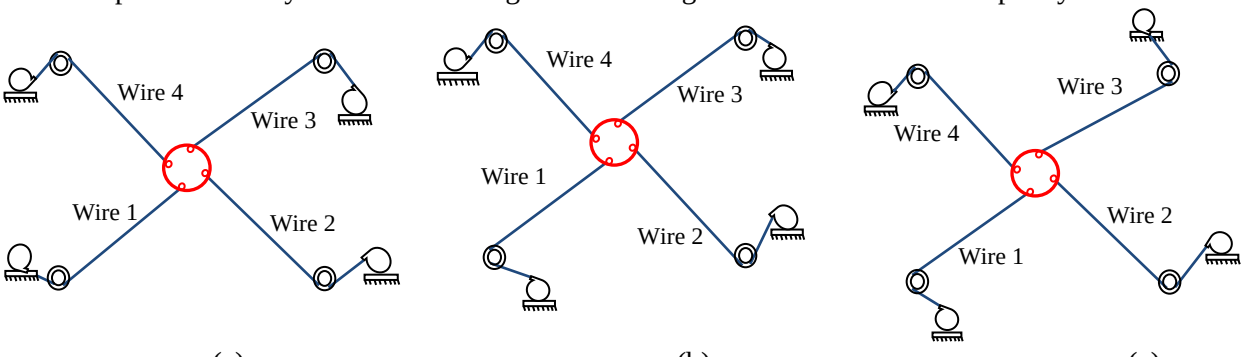

(a) (b) (c)

Fig. 1. Configurations of 4-4 wire-actuated parallel manipulators.

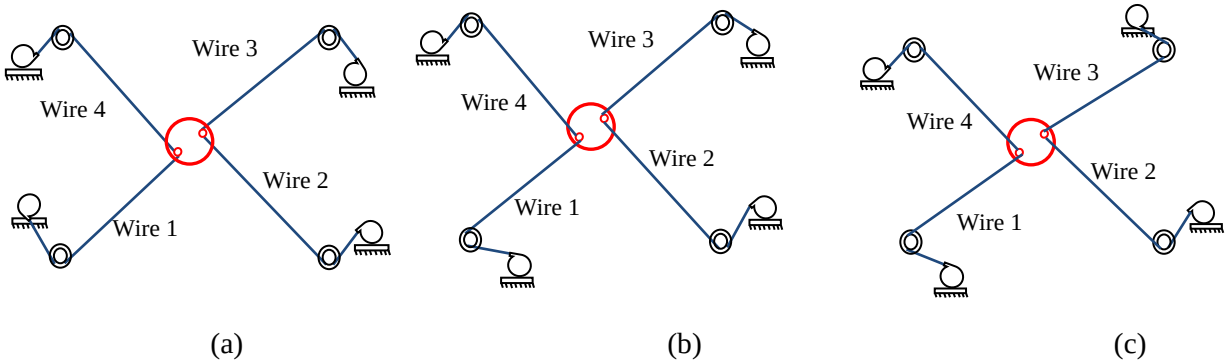

(a) (b) (c)

Fig. 2. Configurations of 2-4 wire-actuated parallel manipulators.

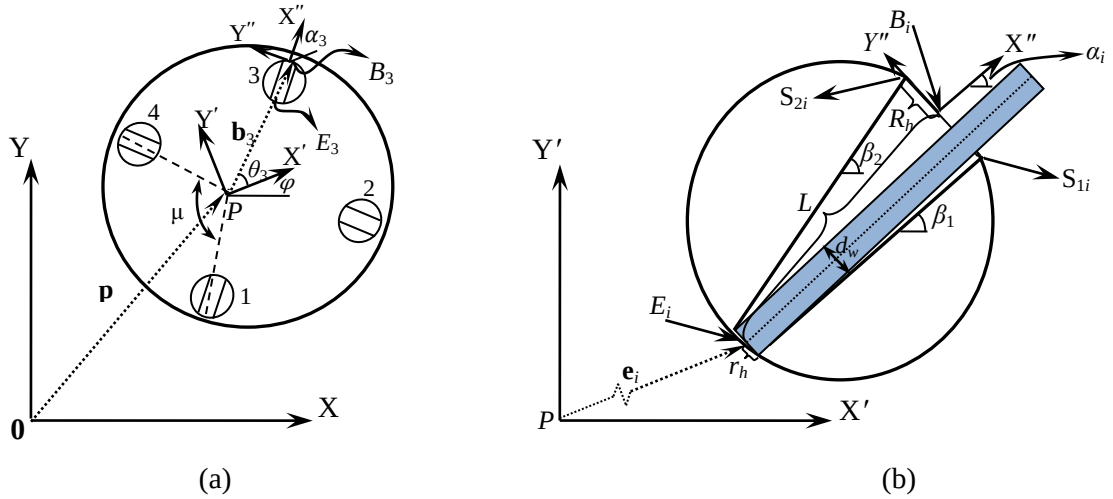

(a) (b)

Fig. 3. (a) Coordinates of base, mobile platform and peg. (b) Coordinates and parameters of mobile platform.

Fig. 3(a) shows the coordinates of the mobile platform and the peg. The base platform has the fixed coordinate system Ψ(X, Y), located at 0, while the mobile platform has a coordinate system Γ(X',Y'), fixed to its center of mass, point *P*; *P* has coordinates $\mathbf{p} = [p_x, p_y]^T$ in Ψ(X,Y). The mobile platform is connected to the base through *n* wires. The coordinate system Φ_i(X",Y"), $i = 1,..., n$ is fixed to the center of the hole of the attachment peg (peg hole for brevity) at the exit point, point B_i. The position vector of point B_i in the coordinate system Γ(X', Y') is $\mathbf{b}_i = [b_{ix}, b_{iy}]^T$. The wire is fixed at the entrance end of the hole at point E_i with coordinates of $\mathbf{e}_i = [e_{ix}, e_{iy}]^T$ in the coordinate system Γ(X', Y'). The attachment points of the wires to their corresponding pulleys, anchor position, are denoted by A_i whose position vector in Ψ(X, Y) is $\mathbf{a}_i = [a_{ix}, a_{iy}]^T$. The orientation of mobile platform with respect to the base coordinate system is given as φ. The orientation of lines $\overline{PB_i}$ and the orientations of the peg axis relative to the coordinate system Γ(X', Y') are represented by angles θ_i and α_i , respectively. The angle between lines $\overline{PB}_1$and $\overline{PB}_4$ and lines $\overline{PB}_2$ and $\overline{PB}_3$ is defined by μ.

2.1 Wire attachment point on mobile platform

The wire attachments on the mobile platform could be in the form of wire attachment pegs. The geometry of the wire attachment peg of [14] is slightly modified to eliminate the uncertainty at which the wire exits the peg hole. That is, the cylindrical hole of the attachment peg is changed into the taper-shaped hole in which the wire is fixed at the entrance end of the hole, E_i, and slides only at the exit point

of the peg hole. Therefore, the uncertainty in wire attachment point to the pulley is removed. The wire rope with diameter of d_W passes through a tapered-shape hole of the attachment peg. The chamfered peg hole, which goes through the wire attachment peg, has the entrance radius r_h and the exit radius R_h, Fig. 3(b). The position of the wire at the peg hole with respect to the coordinate system Φ_i(X",Y") is defined as ${}^{\Phi i}\mathbf{w}_i$. The maximum amount the wire can shift from the center of the peg hole is $(R_h - r_h)$ in Y"-direction. Since the hole at the exit point has a larger radius than the wire, as the mobile platform moves, the wire will be shifted in Y″-direction and the exact point where the central axis of wire exits the hole must be calculated according to the mobile platform pose.

The point at which the wire exits the peg hole is on a plane perpendicular to the plane of the mobile platform. Since the hole is three dimensional, the wire at the exit of the hole can move out of the plane of motion. In this paper, it is assumed that the mobile platform translation in Z-direction and rotation about X-and Y-axes are negligible. Hence, the wire attachment points on the mobile platform are modeled in two dimensions.

It should be noted that the wire fixed to a revolute joint could eliminate the possible uncertainty in the exact position of the wire attachment point on the mobile platform. However, replacing the failed wire using a revolute joint or pulley is not as easy as the one in the proposed attachment peg.

The position of wire i at the peg hole could be calculated relative to the mobile platform and base coordinate systems. For the planar motion, the Z-axis of each coordinate system will be normal to the plane of motion. Therefore, the rotation between any of the two coordinate systems can be described with a single angle about the corresponding Z-axis. The transformation from Φ_i(X",Y") to Γ(X',Y') is given as

$$\mathbf{A}_{\Gamma,\Phi i} = \begin{bmatrix} \cos(\alpha_i) & -\sin(\alpha_i) & b_{ix} \\ \sin(\alpha_i) & \cos(\alpha_i) & b_{iy} \\ 0 & 0 & 1 \end{bmatrix} \tag{1}$$

The transformation from Γ (X', Y') to Ψ(X, Y), matrix $\mathbf{A}_{\Psi,\Gamma}$, has the same form as $\mathbf{A}_{\Gamma,\Phi i}$ except α_i is replaced by φ and b_{ix} and b_{iy} change to p_x and p_y, respectively. $\mathbf{A}_{\Gamma,\Phi i}$ is constant for each attachment point on the mobile platform. Hence, the position of wire center, W_i, at the peg exit with respect to the base coordinate system is $\begin{bmatrix} {}^{\Psi}\mathbf{w}_i^T & 1 \end{bmatrix}^T = \mathbf{A}_{\Psi,\Gamma}\mathbf{A}_{\Gamma,\Phi_i}\begin{bmatrix} {}^{\Phi_i}\mathbf{w}_i^T & 1 \end{bmatrix}^T$.

2.2 Wire attachment point to pulley (anchor position)

The anchor position is the point at which the wire exits the pulley. For a given pose of the mobile platform, the exact point at which the wire exits the pulley can be calculated. Since translation along Z-axis is neglected, the anchor position can be modeled in two dimensions. The constant coordinates of the center of pulley i, D_i, are (d_{ix}, d_{iy}) in the base coordinate system. The formulation of the wire connection points to the mobile platform was discussed in Section 2.1. The X- and Y-coordinates of the anchor position are functions of the position of the corresponding wire attachment point on the mobile platform and the radius of the pulley, r, which are constant. Since the wire will exit tangent to the pulley, a right angle triangle can be formed with points A_i (anchor position), W_i (wire center at the peg exit), and D_i (pulley center) as reported in [14]. Using Pythagorean theorem and Fig. 4(a)

$$\left\| {}^{\Psi}\mathbf{h}_i \right\|^2 = r^2 + \left\| {}^{\Psi}\mathbf{l}_i \right\|^2 \Rightarrow \left(d_{ix} - {}^{\Psi}w_{ix}\right)^2 + \left(d_{iy} - {}^{\Psi}w_{iy}\right)^2 = r^2 + \left(a_{ix} - {}^{\Psi}w_{ix}\right)^2 + \left(a_{iy} - {}^{\Psi}w_{iy}\right)^2 \tag{2}$$

The anchor position is on the circumference of a circle with a known center and radius, i.e.,

$$(a_{ix} - d_{ix})^2 + \left(a_{iy} - d_{iy}\right)^2 = r^2 \tag{3}$$

Solving equations (2) and (3) simultaneously leads to the coordinate of the anchor position, i.e., a_{ix} and a_{iy}. This set of equations has up to two real solutions. Depending on the configuration of the wires, in Fig. 1 and Fig. 2, i.e., clockwise or counter-clockwise winding of wire around the pulley, the suitable solution is chosen. For example, in Fig. 4(a), one of the following possibilities can happen:

1. If the Y-coordinate of the wire attachment point to the mobile platform is equal to the Y-coordinate of the center of pulley, i.e., ${}^{\Psi}w_{iy} = {}^{\Psi}d_{iy}$, and the X-coordinate of the wire attachment point to the mobile platform is greater than the X-coordinate of the center of pulley, i.e., ${}^{\Psi}w_{ix} > {}^{\Psi}d_{ix}$, then the solution with smaller Y-coordinate of the anchor position is chosen for the clockwise winding of wire around the pulley and the larger Y-coordinate is chosen for counter-clockwise winding.
2. If ${}^{\Psi}w_{iy} = {}^{\Psi}d_{iy}$, and ${}^{\Psi}w_{ix} < {}^{\Psi}d_{ix}$, then the greater Y-coordinate of the anchor position is selected for the clockwise winding of wire and the smaller Y-coordinate is chosen for counter-clockwise winding.
3. If ${}^{\Psi}w_{iy} > {}^{\Psi}d_{iy}$, then the solution with the greater X-coordinate of the anchor position is selected for clockwise winding of wire around the pulley and the smaller X-coordinate is chosen for counter-clockwise winding.
4. If ${}^{\Psi}w_{iy} < {}^{\Psi}d_{iy}$, then the solution with the smaller X-coordinate of the anchor position is selected for clockwise winding and the greater X-coordinate is chosen for counter-clockwise winding.

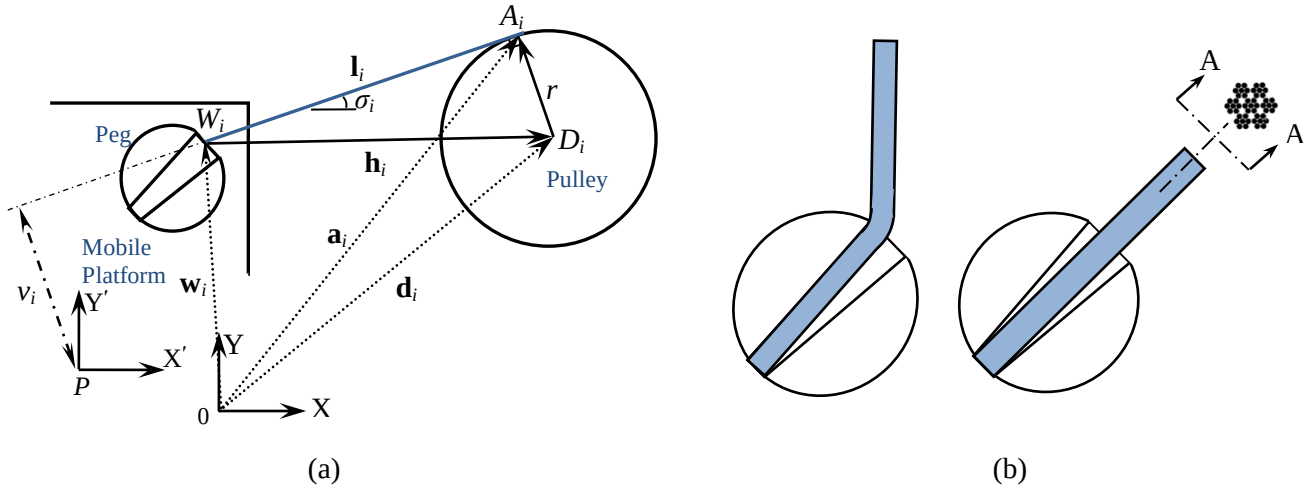

Fig. 4. (a) Coordinates, variables and parameters of peg and pulley. (b) Wire exiting attachment peg with and without bending and cross section of 7×7 strand core steel wire rope.

2.3 Wire bending at the attachment point on mobile platform

The position of the wire while it leaves the peg hole can be calculated using the geometry of the wire and the hole. Angle σ_i is defined as the orientation of the ith wire axis with respect to the base coordinate system Ψ (X, Y). The position vectors of the wire center when the wire touches the edges of the peg hole at the exit, with respect to the peg coordinate system Φ_i(X",Y"),are defined as ${}^{\Phi_i}s_{1i} = [0 \quad -(R_h - r_h)]^T$ and ${}^{\Phi_i}s_{2i} = [0 \quad (R_h - r_h)]^T$. These position vectors are transferred to the base coordinate system using the transformation matrix $\mathbf{A}_{\Psi,\Gamma}\mathbf{A}_{\Gamma,\Phi i}$ which results in $[{}^{\Psi}\mathbf{s}_i^T \quad 1]^T = \mathbf{A}_{\Psi,\Gamma}\mathbf{A}_{\Gamma,\Phi i}[{}^{\Phi i}\mathbf{s}_i \quad 1]^T$. The position vector of the center of the peg hole at the entrance, point E_i, in the peg coordinate system is given as ${}^{\Phi i}\mathbf{e}_i = [-L \quad 0]^T$, where L is the length of the peg hole. Similarly, the position vector of E_i can be expressed in the base coordinate system using $[{}^{\Psi}\mathbf{e}_i^T 1]^T = \mathbf{A}_{\Psi,\Gamma}\mathbf{A}_{\Gamma,\Phi i}[{}^{\Phi i}\mathbf{e}_i^T \quad 1]^T$.

In addition, as can be seen in Fig. 3(b), β_{1i} and β_{2i} are defined as the orientation of the right-hand edge (S_1) and the left-hand edge (S_2) of the peg hole with respect to the X-axis of the base coordinate system

$$\begin{aligned} \beta_{1i} &= \varphi + \alpha_i - \gamma \\ \beta_{2i} &= \varphi + \alpha_i + \gamma \end{aligned} \tag{4}$$

where $\gamma = \tan^{-1}(\frac{R_h - r_h}{L})$ is the angle of tapered hole in the peg.

The exact positions of the edges of the peg hole in the base coordinate system and the center of the pulley, as well as the radius of the pulley, are known. Therefore, by substituting s_{1i} and s_{2i} for w_i in equations (2) and (3), the tangents to the pulley could be determined. At each pose of the mobile platform, the vectors connecting the two edges of the hole to the corresponding anchor position, A_{1i} and A_{2i}, $i = 1, ..., n$, are used to determine the angular position of wires with respect to the X-axis of the base coordinate system, i.e., σ_{1i} and σ_{2i}.

$$\sigma_{1i} = \tan^{-1}(\frac{a_{1iy} - s_{1iy}}{a_{1ix} - s_{1ix}})$$
$$\sigma_{2i} = \tan^{-1}(\frac{a_{2iy} - s_{2iy}}{a_{2ix} - s_{2ix}}) \quad (5)$$

To determine whether the wire contacts the edge of the peg hole or not, the following three possibilities for wire exiting the peg hole are considered, Fig .4(b):

1. Wire leaves the hole with bending and contacts the right-hand edge of the peg hole. For this case, the condition $\sigma_{1i} < \beta_{1i}$ should be satisfied.
2. Wire leaves the hole with bending and contacts the left-hand edge of the peg hole. The condition $\sigma_{2i} > \beta_{2i}$ should be satisfied.
3. Wire leaves the hole without bending. In this case, the conditions $\sigma_{1i} \geq \beta_{1i}$ and $\sigma_{2i} \leq \beta_{2i}$ should be satisfied.

3 WORKSPACE GENERATION

In this section, the static force/moment equations of the manipulators in Fig. 1 and Fig. 2 are formulated. The relationship between the n×1 vector of wire forces, $\boldsymbol{\tau} = [\tau_1 \ldots. \tau_n]^T$, and the 3×1 vector of forces and moment applied on the mobile platform, $\mathbf{F} = \begin{bmatrix} F_{ext_x} & (F_{ext_y} - mg) & M_{ext_z} \end{bmatrix}^T$, in terms of the 3 × n (n > 3) transposed Jacobian matrix $\mathbf{J}^T$ is

$$\begin{bmatrix} F_{ext_x} \\ F_{ext_y} - mg \\ M_{ext_z} \end{bmatrix} = \begin{bmatrix} \cos(\sigma_1) & \ldots & \cos(\sigma_n) \\ \sin(\sigma_1) & \ldots & \sin(\sigma_n) \\ v_1 & \ldots & v_n \end{bmatrix} \begin{bmatrix} \tau_1 \\ \vdots \\ \tau_n \end{bmatrix} = \mathbf{J}^T \boldsymbol{\tau} \quad (6)$$

where σ_i is the angular position of the ith wire with respect to the X-axis of the base coordinate system, $\cos(\sigma_i) = l_{ix}/\|\mathbf{l}_i\|$, $\sin(\sigma_i) = l_{iy}/\|\mathbf{l}_i\|, \mathbf{l}_i = {}^{\Psi}\mathbf{a}_i - {}^{\Psi}\mathbf{w}_i$, $v_i = ({}^{\Psi}w_{ix} - p_x)\sin(\sigma_i) - ({}^{\Psi}w_{iy} - p_y)\cos(\sigma_i)$ is the normal distance from point P to each wire axis, m is the mass of the mobile platform, g = 9.81 m/s^2 is the gravitational acceleration and $\boldsymbol{\tau}$ is the vector of wire tension.

For a manipulator with n wires, the wire tensions τ_i need to be greater than or equal to zero for the mobile platform to be considered in the wrench closure workspace

$$\boldsymbol{\tau} = \mathbf{J}^{\#T}\mathbf{F} + \mathbf{N}\boldsymbol{\lambda} \quad (7)$$

The first term on the right-hand side of equation (7) is the particular solution to achieve the desired wrench and the second term is the homogeneous solution, which is expressed in terms of n×1 matrix $\mathbf{N}$ whose columns span the null space of the transposed Jacobian matrix and is multiplied by an arbitrary scalar $\boldsymbol{\lambda}$. $\mathbf{J}^{\#T} = \mathbf{J}(\mathbf{J}^T\mathbf{J})^{-1}$ is the generalized (Moore-Penrose) inverse. For the planar wire-actuated parallel manipulators of this paper, four wires controlled by motors are used to achieve the three degrees of freedom. Therefore, these manipulators have one degree of actuation redundancy, and hence, there exists infinite choices for the wire tension vector. The value of $\boldsymbol{\lambda}$ is chosen so that the positive wire tension $\boldsymbol{\tau}$ is achieved. Therefore, testing each position and choosing a $\boldsymbol{\lambda}$ that creates $\boldsymbol{\tau}_{\min} \leq \boldsymbol{\tau} \leq \boldsymbol{\tau}_{\max}$ in equation (7) ensures that the position is inside the workspace, this has been referred to as the null space method for formulating the workspace of a wire-actuated parallel manipulator in [14].

4 SIMULATION RESULTS

In this Section, the effect of variations in design parameters on the workspace of the manipulators of Fig. 1 and Fig. 2 is investigated. The changes in the workspace area and shape due to variations and/or uncertainties in the parameters are studied. In other words, the workspace area is plotted when one of the design parameters is varied within the defined range while the other parameters are set to nominal values. The parameters that affect the workspace of the manipulator include: the winding direction of wires on the pulleys; the radius of the pulley; the orientation, radius, and mass of the mobile platform; the peg length; the ratio of the peg radii at the entrance and exit; and the geometric arrangement of wire attachments points on the mobile platform.

For the four-wire-actuated manipulators of Fig. 1 and Fig. 2, the positions of the center of pulleys, D_i, are (–1, –0.75), (1, –0.75), (1, 0.75), (–1, 0.75) m which form a 1.5 m × 2 m rectangle. The nominal values of the position of the peg exit B_i (peg exit center) are set at a constant radius of $\overline{PB_i}$= 100 mm from the center of the mobile platform. The nominal value of the radius of the pulleys, r, is 20 mm, the peg hole length L is 8 mm, the nominal values of the radii of the peg hole at the entrance, r_h , and the exit R_h , are 2.5 mm and 3.75 mm, respectively, and the wire rope diameter, d_w is 5 mm. The angular coordinates of the wire attachment points on the mobile platform, θ_i is {225˚, 315˚, 45˚, 135˚} and the orientations of the corresponding axis of peg holes with respect to the coordinate system Γ(X',Y'), α_i, are set as {225˚, 315˚, 45˚, 135˚}. The minimum wire tension of 5 N and the maximum wire tension of 350 N are used to investigate if the center of the mobile platform is inside the workspace. The increments of 5 mm in the X and Y coordinates of the mobile platform position are used to generate the plots of this section. Table 1 lists the minimum, nominal, and maximum values of the parameters.

Table 1. Parameters of the manipulator in Fig. 1(a).

Manipulator Parameters	**Minimum Value**	**Nominal value**	**Maximum value**
Radius of pulley, r (mm)	0	20	40
Mobile platform Orientation, φ (deg)	0	0	7
Radius of the mobile platform, $\overline{PB_i}$ (mm)	0	100	200
Mass of the mobile platform, m (kg)	0.01	2.6	5.2
Length of the peg, L (mm)	0	8	16
Ratio of exit and entrance peg hole radii, R_h/r_h	1	1.5	1.75

The material used for the mobile platform is Stainless Steel AISI 302-Cold-rolled with yield strength of 520 MPa, ultimate strength of 860 MPa and density of 8190 kg/m^3. For a cylindrical mobile platform with a thickness of h = 0.01 m and radius of $\overline{PB_i}$ = 0.1 m, the nominal value of the mass of the mobile platform will be m = 2.572 kg ≈ 2.6 kg. The wires are assumed to be 7×7 strand core Vinyl-Coated Galvanized Steel wire rope with a breaking strength of 4092 N [18].A safety factor of 12 is used which results in the allowed maximum wire tension of approximately 350 N.

To determine which configuration in Fig. 1 has the largest workspace for the same design parameters, the workspaces of these three manipulators are plotted in Fig. 5(a). The configuration of Fig. 1(a) has the largest workspace compared to the other two configurations of Fig. 1, with notches located close to the pulleys along the vertical portion of workspace envelope. The width of this workspace is larger than the other workspaces plotted in Fig. 5(a) so the notches are visible. A similar result is achieved in Fig. 5(b) for three configurations of Fig. 2. In this section, the effect of manipulator parameters on the workspace of the wire-actuated manipulator of Fig. 1(a) is investigated.

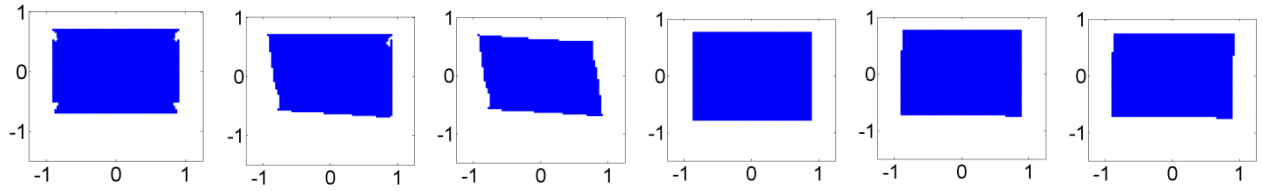

(a) (b)

Fig. 5. Workspaces of six manipulators (a): three layouts in Fig. 1; (b) three layouts in Fig. 2, with nominal values of parameters, without gravity and $\varphi = 0^\circ$.

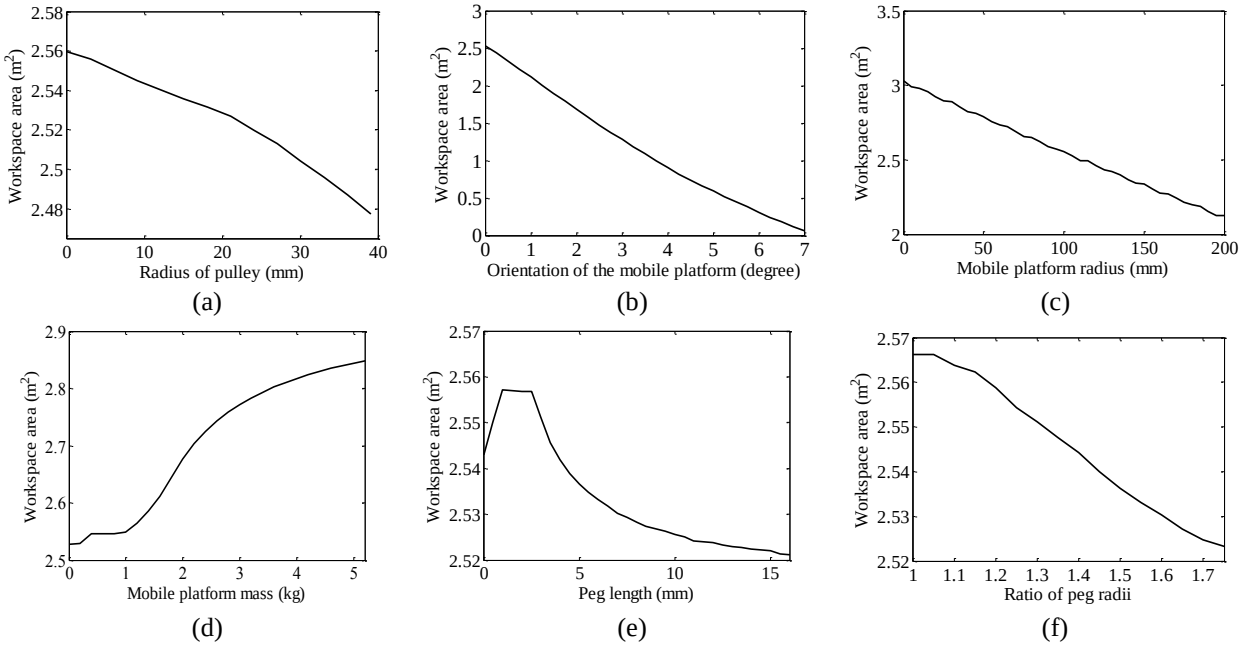

(a) (b) (c)

(d) (e) (f)

Fig. 6. Variation of the workspace area due to change in design parameters.

Plots of Fig. 6 and Fig. 7 show the variation of the workspace area when the parameters of the manipulator of Fig. 1(a) change in the absence of gravity. The cumulative effects of the parameters are reported in Figure 8. Fig. 6(a) depicts the variation of the workspace area when the radius of the pulley changes from 0 to 40 mm and other parameters are set to nominal values. As shown, when the radius of the pulleys increases, the workspace area smoothly decreases, however, the workspace shape is altered by the appearance of notches along the workspace envelope around the pulley location. Fig. 9(a) shows the workspace without gravity for minimum, nominal and maximum values of the radius of the pulley. The notches become larger as the radius of the pulley is increased. In the third plot of Fig. 9(a), the size of the notches is approximately 5 times larger than the radius of the pulley. The top notches are located below the pulleys and the bottom ones are above the pulleys. Therefore, there is a direct relationship between the radius of pulley and the size of the notch. In Fig. 9(b), the results are repeated when the gravity is included and the mass of the mobile platform is 2.6 kg, with a tapering section added to the lower-center of the workspace in the direction of gravity. Due to the effect of gravity, the two notches on the top corners of the workspace become smaller compared to the no gravity cases.

As depicted in Fig. 6(b), the workspace of the manipulator drastically changes as the orientation of the mobile platform changes from 0˚ to 7˚. The workspace shrinks almost linearly from 2.5 m^2 to 0 m^2 while the orientation of the mobile platform increases counter-clockwise. Fig. 10(a) provides the workspace of the manipulator for the cases with $\varphi = 0^\circ$, 3˚and 7˚, respectively when gravity is not considered. In the orientation of 7˚, the rectangular workspace turns into a line which is directed from the upper-left to the

lower-right pulleys. When the mobile platform orientation is increased, the size of the workspace was reduced. Therefore, notches around pulleys would be outside the workspace. It should be noted that if the mobile platform is oriented clock-wise, the area of the workspace is changed in the same fashion but the shape is now directed from the upper-right to the lower-left pulleys. Fig. 10(b) represents the workspace of the manipulator in the presence of gravity. The notches are eliminated for the orientation greater than 0°.In this case, the workspace for the orientation greater than 7° is due to the combined effect of the gravitational force and wires.

Fig. 6(c) shows the effect of the size of the mobile platform on the workspace when the mobile platform radius is changed from 0 to 200 mm. The larger the size of the mobile platform is, the smaller the workspace area will be. When the radius is zero, the mobile platform is considered as a point mass and the orientation of the mobile platform, the peg length, the orientation of peg axis and the ratio of exit and entrance radii of peg hole would not matter. As shown in the plot, for some ranges of the radius, the change in the workspace area is not distinct when the radius is increased. For the workspace investigation, the horizontal and vertical increment for data points is 5×10^{-3} m. Therefore, the accuracy in calculating the area of the workspace is 0.25×10^{-4} m^2. That is, using 4 digits after the decimal point for the workspace area, a change less than 10^{-4} cannot be distinguished. Fig. 11(a) depicts the workspace of the manipulator when the radius of the mobile platform has the minimum, nominal and maximum values. Once the radius of the mobile platform is increased, the workspace and the notches at the corners are decreased. For the mobile platform radius of 0, the notches disappear because the effect of the wire attachment peg vanishes. The results are repeated in Fig. 11(b) when gravity is included.

The mass of the mobile platform affects the workspace when gravity is included. Fig. 6(d) indicates that increasing the mass of the mobile platform from 0 to 5.2 kg increases the workspace area. An increase in the mass of the mobile platform from 0 to 0.2 kg and 0.4 kg to 0.8 kg leads to a slight increase in the workspace which is not distinguishable as a result of the defined resolution for workspace area, i.e., changes less than $10^{-4}m^2$ cannot be shown in Fig. 6(d). In Fig. 12, the workspace is plotted when m = 0.01, 1, 2.6, and 5.2 kg, respectively. As the mass (weight) increases, the thickness of the tapered section, and hence the workspace below the lower anchors, which exists due to gravity, increases. The tapered section in the lower-center of the workspace does not grow enough for m = 1 kg, however a small change in the workspace of the manipulator is introduced compared to the case of m = 0.01 kg. This section is noticeably extended downward for m = 2.6 kg.

In Fig. 6(e), the variation of the workspace area when the length of the peg changes from 0 to 16 mm is represented, which is much smaller compared to the effect of other parameters. While the length of the peg increases from 0 to 1 mm, the workspace increases and reaches the maximum value at L = 1 mm. Then increasing the peg length from L = 1 mm to L = 2.5 mm leads to a slight decrease in the workspace. Further increase of the peg length results in a sharper decrease in the workspace. As shown in Fig. 6(e), the variation of the peg length has a relatively minor effect on the workspace area of the mobile platform. The plots of Fig. 13 depict the workspace of the manipulator for the cases of L = 1, 8 and 16 mm. It is shown that longer peg hole increases the size of the notches.

In Fig. 6(f) the variation of the workspace when the ratio of the exit and entrance peg hole radii changes from 1 to 1.75 is given. When this ratio increases, the workspace area slightly decreases. The workspaces of the manipulator when all parameters, except the ratio of the peg radii, have nominal values without and with gravity are depicted in Fig. 14(a) and Fig. 14(b), respectively. The larger the ratio of the peg radii is, the larger the size of the notches along the workspace envelope will be. However, the effect of gravity reduces the size of the notches at the upper section of the workspace.

The plots of Fig. 6 showed the effect of design parameters on the workspace of a 4-4 layout (with four distinct wire attachment points). As depicted in Fig. 3(a), the peg exit centers B_i are located at the corners of a square, i.e., lines $\overline{PB}_2$ and $\overline{PB}_3$, and $\overline{PB}_1$ and $\overline{PB}_4$ form right angles ($\mu = 90^\circ$). To study the change in the workspace area when the wire attachment points on the mobile platform are varied from the 4-4 wire

layout (Fig. 1(a)) to the 2-4 wire layout (Fig. 2), angle μ is varied from 90˚ to 0˚. The orientation of the peg axis is set to be aligned with the angular position of $\overline{PB_i}$ and the orientation of the mobile platform is φ = 7˚.As shown in Fig. 8(a), the manipulator has no workspace when angle μ changes from 89˚ to 62˚ and the workspace increases as μ changes from 62˚ to 0˚. Fig. 15 shows the workspace of the manipulator when μ is 61˚, 45˚ and 0˚ without and with gravity. The case of the 4-4 wire layout (μ = 90˚) corresponds to the third plots in Fig. 10(a) and Fig. 10(b) when φ = 7˚ without and with gravity, respectively.

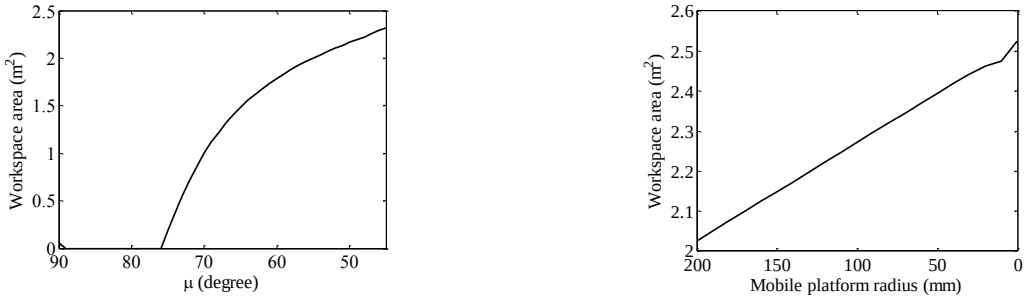

(a) (b)

Fig. 7. Variation of workspace when: (a) mobile platform changes from 4-4 wire layout to 2-4 wire layout; (b) mobile platform changes from 2-4 wire layout to a point without gravity.

(a) (b)

Fig. 8. Workspace of manipulator in Fig. 1(a) for: (a) minimum values of parameters without (left) and with gravity (right); (b) maximum values of parameters without (left) and with gravity (right).

To study how the workspace of the manipulator changes if the mobile platform is altered from a 2-4 wire layout to a point mass, the plot in Fig. 8(b) is prepared when the orientation of the mobile platform is 7˚. As the radius of the mobile platform decreases, the workspace area increases from 2 m^2 to 2.53 m^2.

The cumulative effects of the parameters, i.e., the pulley radius, the mobile platform radius, the peg length, and the ratio of peg hole radii on the shape and size of the workspace for φ = 0˚ are reported in Fig. 8. Fig. 8(a) and Fig. 8(b) respectively depict the plots of the workspace for the minimum and maximum values of aforementioned parameters without and with gravity. As it was discussed for Fig. 6, an increase in each parameter from minimum to maximum value led to a decrease in the workspace area and also the appearance of notches. The overall increase in the parameters decreases the area of the workspace and increases the size of the notches along the workspace envelope.

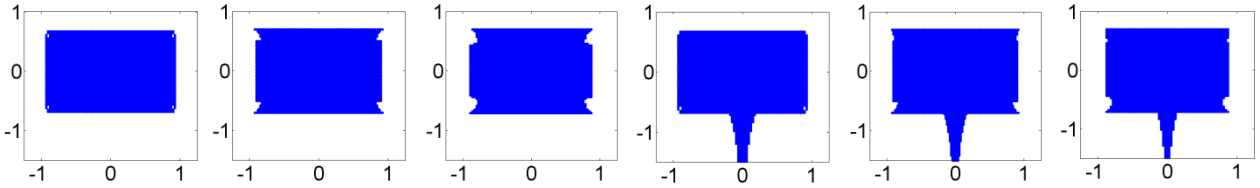

(a) (b)

Fig. 9. Workspace of manipulator in Fig. 1(a) as a function of pulley radius: (a) without gravity; (b) with gravity.

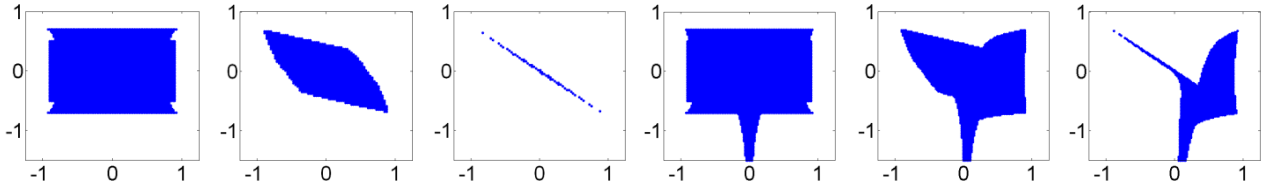

Fig. 10. Workspace of manipulator in Fig. 1(a) as a function of mobile platform orientation: (a) without gravity; (b) with gravity.

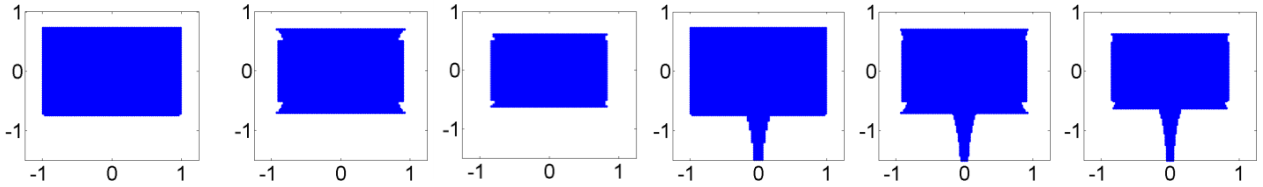

Fig. 11. Workspace of manipulator in Fig. 1(a) as a function of mobile platform radius: (a) without gravity; (b) with gravity.

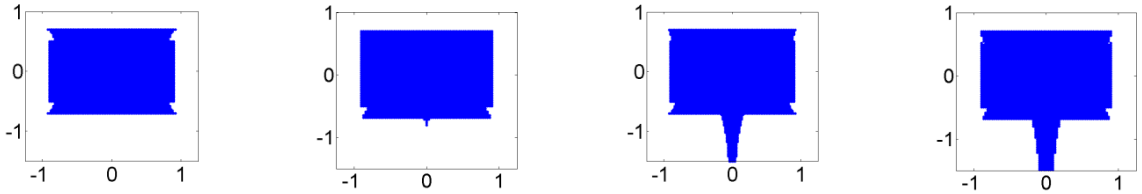

Fig. 12. Workspace of manipulator in Fig. 1(a) as a function of mobile platform mass.

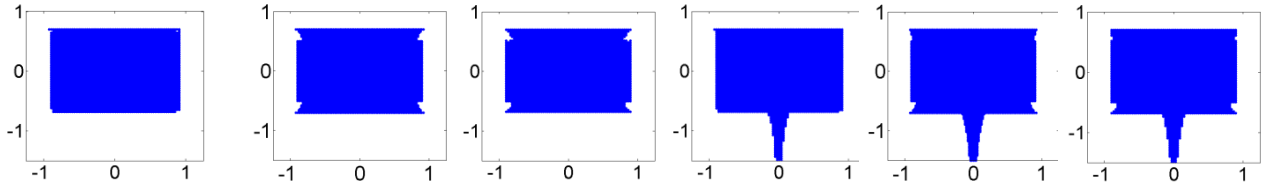

Fig. 13. Workspace of manipulator in Fig. 1(a) as a function of peg length: (a) without gravity; (b) with gravity.

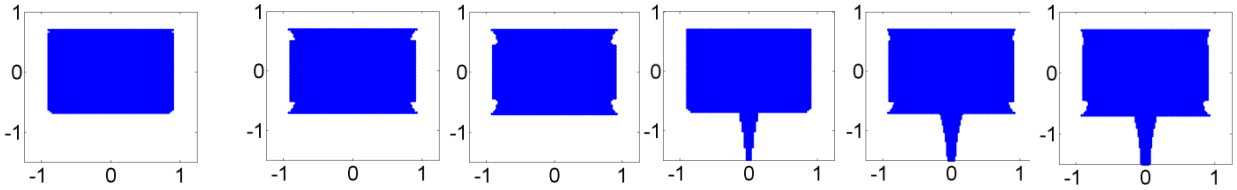

Fig. 14. Workspace of manipulator in Fig. 1(a) as a function of the ratio of peg hole radii: (a) without gravity; (b) with gravity.

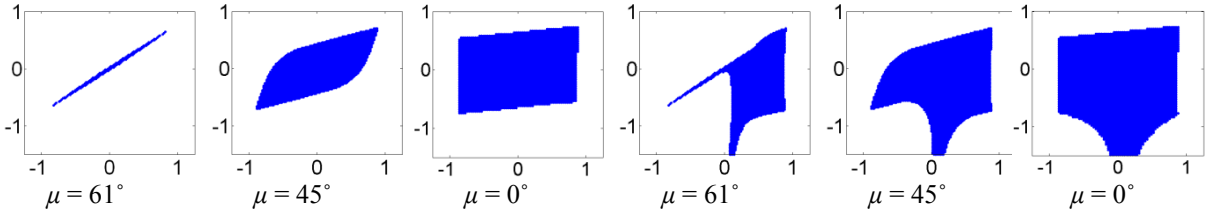

Fig. 15. Workspace of manipulator when the configuration changes from 4-4 wire layout to 2-4 wire layout with nominal values of parameters and $\varphi = 7^{\circ}$: (a) without gravity; (b) with gravity.

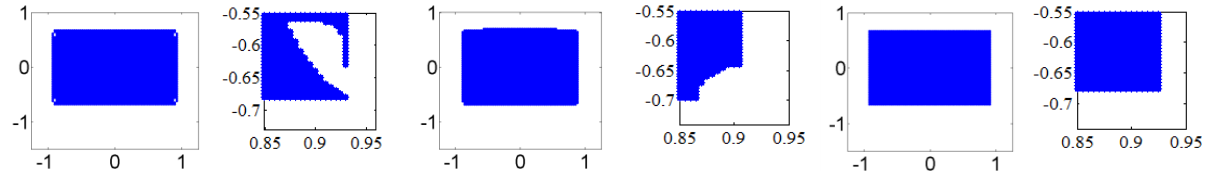

Fig. 16. Effect of peg and pulley on the workspace of the manipulator in Fig. 1(a) when $\varphi = 0^{\circ}$ with nominal value of $\overline{PB}_i$ = 100 mm and without gravity: (a)-(b) r = 0; (c)-(d) L = 0; (e)-(f) r = 0, L = 0.

The effect of the mobile platform peg and the pulley on the shape and size of the workspace is presented in Fig. 16. In Fig. 16(a), the radius of pulley is zero (r = 0) and the effect of the peg on the size and shape of the workspace is investigated for the manipulator in Fig. 1(a) without gravity when $\varphi = 0^{\circ}$. There still exist notches along the workspace envelope around the pulley locations. Fig. 16(b) depicts a close-up view of the lower-right section of the workspace. In Fig. 16(c), the wire attachment on the mobile platform is taken as a point (zero peg length, L = 0) and the effect of the pulley on the shape and size of workspace is considered. The workspace area in Fig. 16(a) is larger than that in Fig. 16(c) and the depth of notches noticeably reduces as shown in Fig. 16(d). In Fig. 16(e), the effect of the peg and the pulley on the workspace is removed (r = 0 and L = 0). As shown in Fig 16(e) and Fig. 16(f), the notches are completely eliminated. Compared to the pulleys, the wire attachment pegs on the mobile platform introduce larger notches around the pulleys.

6 DISCUSSION AND CONCLUSION

In this paper, the effect of variations in design parameters on the workspace size and shape of the wire-actuated parallel manipulators without and with gravity was investigated. These parameters include: the winding direction of wires on pulleys, the radius of the pulleys; the orientation, radius, and mass of the mobile platform; the peg length; the ratio of the peg radii at the entrance and exit; and the geometric arrangement of wire attachment points on the mobile platform. Generally, in 4-4 wire layouts, the workspace area was decreased as the radius of the pulleys, the orientation and the radius of the mobile platform, and the ratio of the peg hole radii were increased one at a time. When the gravity was included, an increase in the mass of the mobile platform led to an increase in the workspace area and introduced a downward tapered section at the lower-center of the rectangular workspace, and increased the thickness of tapered section. The shape of the workspace was also affected while the design parameters were changed. When the radius of the pulleys, the peg length, and the ratio of the peg hole radii were increased, the rectangular shape of the workspace was maintained. However, notches appeared along the vertical portion of the workspace envelope close to the pulley locations and the size of notches was increased. As the radius of the mobile platform was increased, the shape of the workspace was maintained while the size of the workspace was reduced which resulted in reduction in the size of notches.

The shape of workspace was changed from rectangular to a diagonal line when the orientation of the mobile platform was increased from zero to the maximum value of 7°. When the mobile platform

configuration was altered from a 4-4 wire layout to a 2-4 wire layout for a mobile platform orientation of 7˚, the workspace was changed from a line to a parallelogram. When the mobile platform was altered from a 2-4 wire layout to a point mass, the workspace area was increased. As the future work, the effect of the design parameters on the failure recovery performance of wire-actuated parallel manipulators could be studied. In addition, once an accurate workspace is identified, the effect of the design parameters on the velocity control could be investigated.

REFERENCES

1. Bostelman R., Albus J., Dagalakis N., Jacoff A., and Gross J.L., Applications of the NIST Robocrane, *Robotics and Manufacturing*, Vol. 5, pp. 403–410, 1994.
2. Roberts R.G., Graham T., and Lippitt T., On the Inverse Kinematics, Statics, and Fault Tolerance of Cable-Suspended Robots, *J. of Robotics Sys.*, Vol. 15, No. 10, pp. 581–597, 1998.
3. Kawamura S., and Ito K., New Type of Master Robot for Teleopertaion Using a Radial Wire Drive System, *IEEE/RSJ Int. Conf. on Intelligent Robots and Systems*, Yokohama, Japan, pp. 55–60, 26-30 July 1993.
4. Fattah A., and Agrawal S. K., Workspace and Design Analysis of Cable-suspended Planar Parallel Robots, *ASME Design Engineering Technical Conf., 27th Biennial Mechanisms and Robotics Conf., DETC2002/MECH-34330*, Montreal, Canada, 29 September-2 October, 2002.
5. Barrett G., and Gosselin C. M., Kinematic Analysis and Design of Planar Parallel Mechanisms Actuated with Cables, *ASME Design Engineering Technical Conf., DETC/MECH-14091*, Baltimore, USA, 2000.
6. Ferraresi C., Paoloni M., and Pescarmona F. A., New Methodology for the Determination of the Workspace of Six-DOF Redundant Parallel Structures Actuated by Nine Wires, *Robotica*, Vol. 25, No. 1, pp. 113–120, 2006.
7. Williams R.L. II., and Gallina P., Planar Cable-Direct-Driven Robots: Design for Wrench Exertion, *J. of Intelligent and Robotics Systems*, Vol. 35, No. 2, pp. 203–219, 2002.
8. Oh S.R., and Agrawal S.K., Cable Suspended Planar Robots with Redundant Cables: Controllers with Positive Tensions, *IEEE Trans. on Robotics*, Vol. 21, No. 3, pp. 457–465, 2005.
9. McColl D., and Notash L., Configuration and Workspace Analysis of Planar Wire-Actuated Parallel Manipulators, *17th CISM-IFToMM Symp. Robot Design, Dynamics, and Control (RoManSy*), Tokyo, Japan, 8 pages, July 2008.
10. Pham C.B., Yeo S.H., Yang G., Kurbanhusen M.S., and I-Ming C., Force-closure Workspace Analysis of Cable-driven Parallel Mechanisms, *Mech. and Mach. Theory*, Vol. 41, No. 1, pp. 53–69, 2006
11. Diao X., and Ma O., Force-Closure Analysis of General 6-DOF Cable Manipulators, *IEEE/RSJ Int. Conf. on Intelligent Robots and Systems*, San Diego, USA, pp. 3931–3936, 29 October- 2 November 2007.
12. Gouttefarde M., and Gosselin C. M., Analysis of the Wrench-Closure Workspace of Planar Parallel Cable-Driven Mechanisms, *IEEE Trans. on Robotics*, Vol. 22, No. 3, pp. 434–445, 2006.
13. Stump E., and Kumar V., Workspaces of Cable-Actuated Parallel Manipulators, *ASME J. of Mechanical Design*, Vol. 128, No. 1, pp. 159–167, 2006.
14. McColl, D., and Notash, L., Workspace Formulation of Planar Wire-Actuated Parallel Manipulators, *Robotica*, Vol. 29, No. 4, pp. 607–617, 2011.
15. Pusey J., Fattah A., Agrawal S., and Messina E., Design and Workspace Analysis of a 6–6 Cable-suspended Parallel Robot, *Mech. and Mach. Theory*, Vol. 39, No. 7, pp. 761–778, 2004.
16. Hay A. M., and Snyman J. A., Optimization of a Planar Tendon-driven Parallel Manipulator for a Maximal Dexterous Workspace, *Engineering Optimization*, Vol. 37, No. 3, pp. 217–236, 2005.

17. Notash L., and McColl, D., Workspace Investigation of Wire-Actuated Parallel Manipulators with Uncertainties in Wire Connections, *ASME 34th Annual Mechanisms and Robotics Conf.*, IDETC/CIE 2010, Montreal, 15–18 August 2010.
18. McMaster-Carr Supply Company, issue 118, pp. 1409, Atlanta, Georgia, 2012.